Stress–Strain Distribution Analysis in Bi2212 Subcable Based on Numerical Modeling and Experiment

Jinggang Qin, Chao Dai, Qiuliang Wang, *Member, IEEE*, Peihang Liu, Bo Liu, Chenshan Li, Qingbin Hao, and Chao Zhou

***Abstract*—There has been sustained interest in the development of the Bi2212/Ag round wire (RW) because of its unique potential for applications in high-field magnets (25 T or higher). The Bi2212 conductor is a round strand, which is a very favorable shape to produce multistage twisted cable-in-conduit conductors (CICCs) for the next fusion machine (DEMO). One drawback of Bi2212 is its fragile mechanical properties. The stress and strain accumulated during cabling, the thermal contraction during cooldown, and the electromagnetic load can have a severe impact on the transport properties of the Bi2212 RW. In order to investigate the strain distribution of Bi2212 in CICC, some research and development work was made at the Institute of Plasma Physics, Chinese Academy of Sciences (ASIPP). A simple cable wound with three Bi2212 RWs was manufactured and subjected to mechanical tests. A numerical model was proposed to analyze the stress–strain distribution of a wire inside a cable at cryogenic temperature. Comparisons were made between the model and experimental results. Based on the results and improved understanding of the mechanical behavior, an optimization could be implemented to reduce the Bi2212 cable degradation, in terms of conductor design, manufacture, and operation.**

***Index Terms*—Bi2212 cable, experiment, numerical model, strain.**

I. Introduction

HIGH upper critical (B_{c2}) fields and irreversibility fields ($B_{\rm irr}$) are needed for new magnets, which can be operated near or even above the B_{c2} limit of Nb_3Sn. The critical current density of low-temperature superconducting conductors such as Nb_3Sn decreases rapidly with increasing field in the 15- to 25-T range, whereas the Bi2212 field dependence is relatively constant in this range, making it promising for application in high-field magnets [1]–[3]. Bi2212 is presently also the only cuprate superconductor that can be made into round wire (RW). This makes it possible to develop a Bi2212 cable-in-conduit conductor (CICC) [4], [5], which can be used for the next generation of fusion magnets, reaching higher field than ITER [6], [7]. The magnet with the highest field in a tokamak fusion reactor is subjected to tens of thousands of electromagnetic load cycles at several tens of megapascal peak Lorentz force. Therefore, analysis of the mechanical properties is essential, and impact on cable design, manufacturing, and operation at low temperature needs more investigation.

Several models [8]–[10] have been introduced to analyze the cable pattern for Nb3Sn or NbTi CICC, including cabling and conductor operation at low temperature. Large tension on strands and cable can cause undesired single-strand elongation or damage during cabling. Inappropriate axial tension on strands can cause differences in the strain of the strands made from different materials, possibly resulting in kinks and an unengaged cable. The Bi2212 phase is very brittle, and the sheath made of Ag/Ag-Mg alloy has high plasticity and low strength. This combination of mechanical properties can easily lead to a low electromechanical performance in terms of electrical current transport properties [11], [12]. The Bi2212 wire is sensitive to strain, and strain can easily lead to cracks that cause a significant irreversible reduction of the critical current density J_c [13]. For the Bi2212 cable, only little research has been performed on its mechanical properties.

In this paper, the results of investigations on a cable made of three single Bi2212 RWs with different pitches subjected to tensile stress–strain tests at 300 K are reported. The mechanical properties were analyzed by a numerical cable model [10]. The experimental results were compared with the numerical model for conditions at 300 K. Then, the model was used to analyze the strain distribution of a single wire in different cable configurations at room and cryogenic temperatures. The numerical and experimental results are not only important for the analysis of cable design and operation but may also even be essential for the improvement of the cabling technique.

II. Numerical Model

A. Basic Definitions

In the Cartesian coordinate system ($X-Y-Z$), the Z-axis coincides with the center line of the cable. The local coordinate

Manuscript received June 23, 2015; revised September 21, 2015, February 3, 2016, February 25, 2016, and February 29, 2016; accepted February 29, 2016. Date of publication March 23, 2016; date of current version April 15, 2016. This work was supported in part by the National Magnetic Confinement Fusion Science Program under Grant 2013GB110001 and in part by the National Natural Science Foundation of China under Grant 51207157. This paper was recommended by Associate Editor L. Chiesa.

J. Qin is with the Institute of Electrical Engineering, Chinese Academy of Sciences, Beijing 100190, China, and also with the Institute of Plasma Physics, Chinese Academy of Sciences, Hefei 230031, China (e-mail: qinjg@ipp.ac.cn).

C. Dai, P. Liu, B. Liu, and C. Zhou are with the Institute of Plasma Physics, Chinese Academy of Sciences, Hefei 230031, China.

Q. Wang is with the Institute of Electrical Engineering, Chinese Academy of Sciences, Beijing 100190, China.

C. Li and Q. Hao are with the Northwest Institute for Non-ferrous Metal Research, Xi'an 710016, China.

Color versions of one or more of the figures in this paper are available online at http://ieeexplore.ieee.org.

Digital Object Identifier 10.1109/TASC.2016.2544824

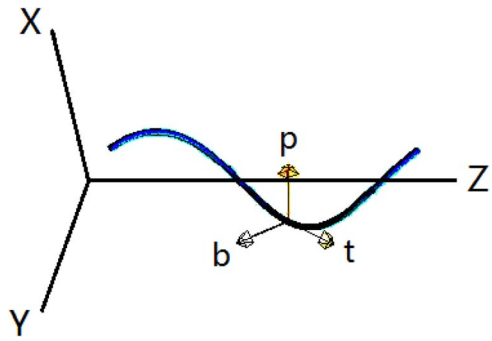

Fig. 1. Coordinate systems.

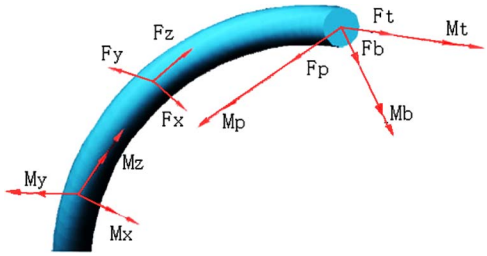

Fig. 2. Loading acting on rod.

system is formed by the Frenet frame $(p-b-t)$ with unit principal normal, binormal, and tangent vectors, as shown in Fig. 1.

B. Thin Rod Theory

For the convenience of the reader, this section reviews the thin rod theory [14].

A thin wire loaded with force, as shown in Fig. 2, was considered. Let s be the arc length along the wire. F_p, F_b, and F_t are the sectional force components of the wires, and M_p, M_b, and M_t are the sectional moment components of the wires. F_x, F_y, and F_z are the components of the external line load, and M_x, M_y, and M_z are the components of the external moment.

The equilibriums of the loaded thin rod can be obtained from the following:

$$\frac{dF_p}{ds} - F_b\kappa_t + F_t\kappa_b + F_x = 0 \tag{1}$$

$$\frac{dF_b}{ds} - F_t\kappa_p + F_p\kappa_t + F_y = 0 \tag{2}$$

$$\frac{dF_t}{ds} - F_p\kappa_b + F_b\kappa_p + F_z = 0 \tag{3}$$

$$\frac{dF_p}{ds} - M_b\kappa_t + M_t\kappa_b - F_b + M_x = 0 \tag{4}$$

$$\frac{dM_b}{ds} - M_t\kappa_p + M_p\kappa_t + F_p + M_y = 0 \tag{5}$$

$$\frac{dM_t}{ds} - M_p\kappa_b + M_b\kappa_p + M_z = 0 \tag{6}$$

where κ_p, κ_b, and κ_t are the curvature components.

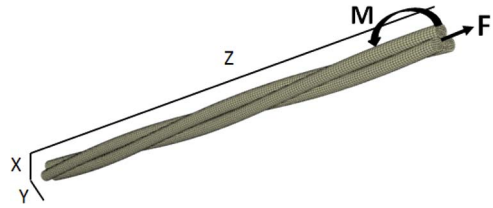

Fig. 3. Cable under tension and torsion.

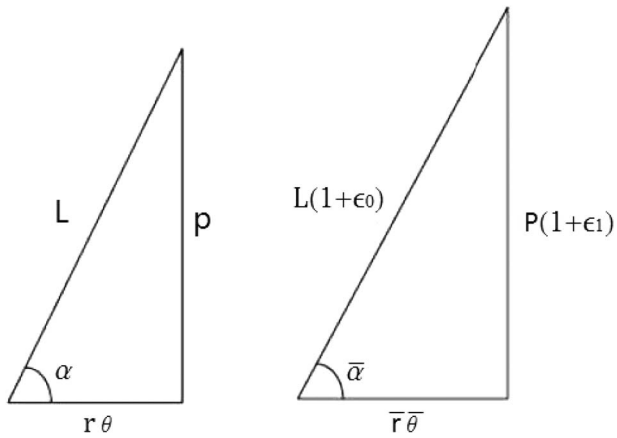

Fig. 4. Developed view of the single wire [(left) without strain; (right) with strain under tension].

C. Numerical Model for Bi2212 Cable Under Loading

Here, the model is given for wires in a triplet, which is under axial force and torsion, as shown in Fig. 3.

The parameter equation of the single wire is given as follows:

$$X = r\cos\theta \tag{7}$$

$$Y = r\sin\theta \tag{8}$$

$$Z = r\theta\tan\alpha \tag{9}$$

where r is the twist radius, $\alpha = \arctan(2\pi r/p)$, $\alpha \in (0, \pi/2)$, and p is the twist pitch.

The developed view of a single wire in the cable is shown in Fig. 4. The axial strain of the cable is defined as ϵ_1, and the rotational strain of one single wire is defined as

$$\gamma_1 = r\frac{\overline{\theta} - \theta}{p}. \tag{10}$$

Using standard geometric relations of angles in the defined triangles, we can obtain the equations from Fig. 4 as

$$\epsilon_1 = (1+\epsilon_0)\frac{\sin\overline{\alpha}}{\sin\alpha} - 1 \tag{11}$$

$$\gamma = \frac{r}{\overline{r}}\frac{1+\epsilon_1}{\tan\overline{\alpha}} - \frac{1}{\tan\alpha}. \tag{12}$$

The original components of the curvature and the twist per unit length of a single wire are

$$\kappa_{p_0} = 0 \quad \kappa_{b_0} = \frac{\cos^2\alpha}{r} \quad \kappa_{t_0} = \frac{\sin\alpha\cos\alpha}{r}.$$

The components of the curvature and the twist per unit length of a single wire under load are

$$\overline{\kappa}_{p_0} = 0 \quad \overline{\kappa}_{b_0} = \frac{\cos^2 \overline{\alpha}}{\overline{r}} \quad \overline{\kappa}_{t_0} = \frac{\sin \overline{\alpha} \cos \overline{\alpha}}{\overline{r}}.$$

A wire is considered as a thin rod, and the sectional moments are related to the changes of curvature and torsion. The moments of a single wire can be obtained with

$$M_p = \mathrm{EI}_p(\overline{\kappa}_{p_0} - \kappa_{p_0}) \tag{13}$$

$$M_b = \mathrm{EI}_b(\overline{\kappa}_{b_0} - \kappa_{b_0}) \tag{14}$$

$$M_t = \mathrm{EI}_t(\overline{\kappa}_{t_0} - \kappa_{t_0}) \tag{15}$$

where E is the Young's modulus.

The axial force in the single wire is given by

$$F_t = A_0 \sigma(\epsilon_0) \tag{16}$$

where A_0 is the cross section of the wire, and $\sigma(\epsilon_0)$ is the stress–strain function, which can be obtained from the tensile test of a single wire.

According to the preceding equilibrium, the sectional shear forces and contact force can be expressed by

$$F_p = -\frac{dM_b}{ds} + M_t \cdot \kappa_{p_0} - M_p \cdot \kappa_{t_0} \tag{17}$$

$$F_b = \frac{dM_p}{ds} - M_b \cdot \kappa_{t_0} + M_t \cdot \kappa_{b_0} \tag{18}$$

$$F_x = F_b \cdot \kappa_{t_0} - F_t \cdot \kappa_{b_0}. \tag{19}$$

The total axial force F and the total axial twisting moment M acting on the cable can be obtained by

$$F = 3(F_t \sin \alpha + F_b \cos \alpha) \tag{20}$$

$$M = 3(M_t \sin \alpha + M_b \cos \alpha + F_t r \cos \alpha - F_b r \sin \alpha). \tag{21}$$

The system of equations (16)–(21) can be used to investigate the stress and strain of a single wire when the cable is subjected to a combination of tensile and twisting load.

III. Sample Preparation

Bi2212 RW samples were manufactured using the powder-in-tube method by the Northwest Institute for Non-ferrous Metal Research (NIN). The wire contains 19 × 18 Bi2212 filaments, and the outer sheath of the wire is made of Ag-0.2 wt% Mg alloy. The heat treatment procedure of the Bi2212 RW is with a maximum temperature of 890 °C for 30 min in an oxygen environment. The cross-sectional micrographs are shown in Fig. 5, and the basic parameters of the wire are listed in Table I. Two different types of wire were used for cabling. One is unreacted, and the other is reacted.

Three cables, each with three strands, having twist pitches of 20, 40, and 60 mm, respectively, were prepared, as shown in Fig. 6. During cabling, the tension on the wires was fixed below 10 N in order to avoid damage of the wire.

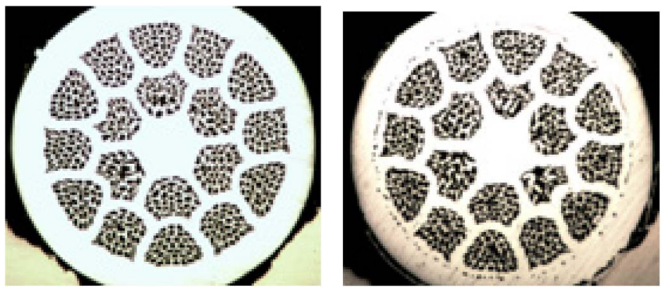

Fig. 5. Cross section of the Bi2212 wire [(left) unreacted; (right) after reaction].

TABLE I
PARAMETERS OF THE TESTED Bi2212 WIRE

Material	Ag-alloy sheathed Bi-2212
Diameter	1.0 mm
Filament configuration	19 x 18
Ag/Mg:Ag:Bi2212	1.8:1:0.9
I_c at 0 T, 4.2 K	about 400 A
I_c at 12 T, 4.2 K	about 146 A

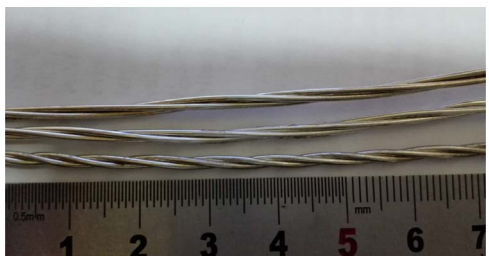

Fig. 6. Cable with different pitches.

IV. Numerical and Experimental Results

A. Mechanical Properties of a Single Wire

The input parameters of the numerical model were obtained from the results of a tensile test on a single wire. The unreacted Bi2212 wire was only tested at 300 K since the mechanical properties of unreacted strand at 300 K are required for the manufacture of the Bi2212 cable. In order to understand the mechanical properties of the Bi2212 wire in the cable after reaction, reacted wire samples were tested at 300, 77, and 4.2 K. The stress strain curves are shown in Figs. 7 and 8.

The results show that the strength of the reacted wire decreases noticeably compared with that of the unreacted wire. The strength of the wire also shows a considerable influence of the temperature, increasing with reducing temperature, as shown in Fig. 8 and Table II [15].

The cable samples were tested only at 300 K.

B. Comparison Between the Numerical and Experimental Results

The function of the stress–strain relation is required as input for the numerical simulation. The fitting functions were given as follows.

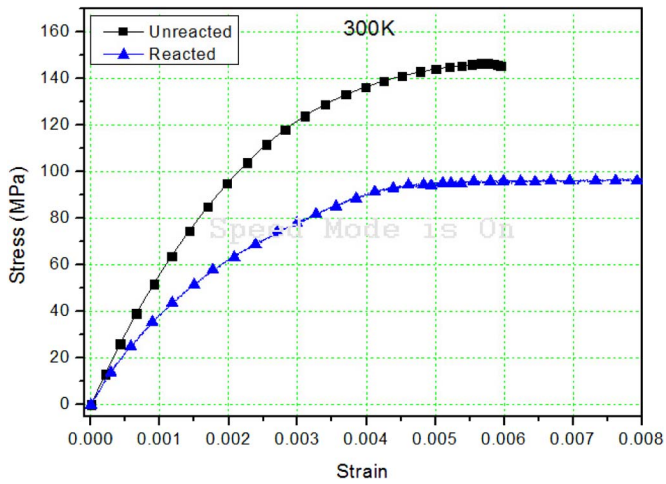

Fig. 7. Stress–strain curves of the reacted and unreacted Bi2212 wires at 300 K.

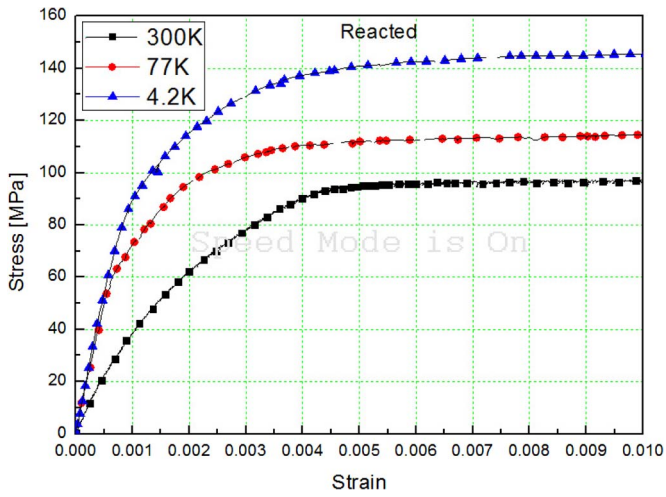

Fig. 8. Stress–strain curves of the reacted Bi2212 wire at 300, 77, and 4.2 K.

TABLE II
PARAMETERS OF NUMERICAL MODELING

State	Temperature	Yield Strength/MPa	Young's Modulus/GPa
Unreacted	300 K	146	65
Reacted	300 K	126	55
Reacted	77 K	107	106
Reacted	4.2 K	217	116

The fitting function for the unreacted wire at 300 K is

$$\sigma(x) = (-2.6165 + 66845.20851x - 4.9268 \times 10^6 x^2 - 5.67051 \times 10^8 x^3 + 6.45802 \times 10^{10} x^4) \times 10^6. \quad (22)$$

The fitting function for the reacted wire at 300 K is

$$\sigma(x) = \left(92.51456 - 32.8361 e^{\frac{-x}{0.00572}} - 61.07028 e^{\frac{-x}{0.00101}}\right) \times 10^6 \quad (23)$$

where σ is the stress (MPa), and x is the strain.

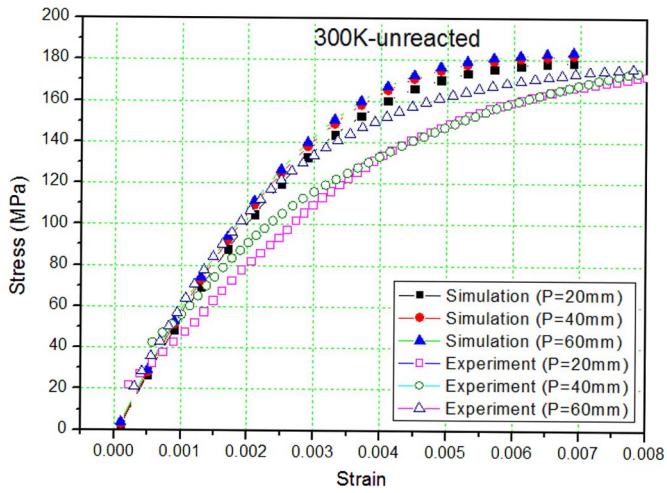

Fig. 9. Stress–strain curves of the unreacted cables at 300 K.

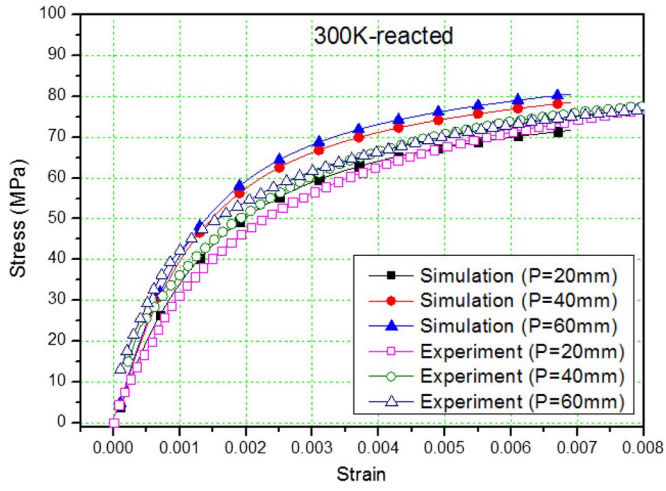

Fig. 10. Stress–strain curves of the reacted cables at 300 K.

Using (17)–(21), the stress–strain curves of the cable under tension can be obtained. The results are compared with the experiments in Figs. 9 and 10.

For the stress–strain curves of the reacted cables, the agreement between the numerical and experimental results is good, particularly for the cable with a 20-mm-long twist pitch. The simulation for the unreacted cables does not match well with the experimental results. The deviation may be caused by the neglected contact deformation. For the unreacted wire, more contact force exists in the wires, which could cause more deformation. The results shown in Figs. 9 and 10 illustrate that the stress needed to reach a certain strain level of the cable increases with enlarged pitch, which was also demonstrated by the experimental results.

C. Strain Analysis on a Single Wire of the Cable

During cabling at room temperature and operation at low temperature, the cable is subjected to tension or contraction. As a consequence, the single wires will experience strain because of the cable tension, with the possible risk of wire

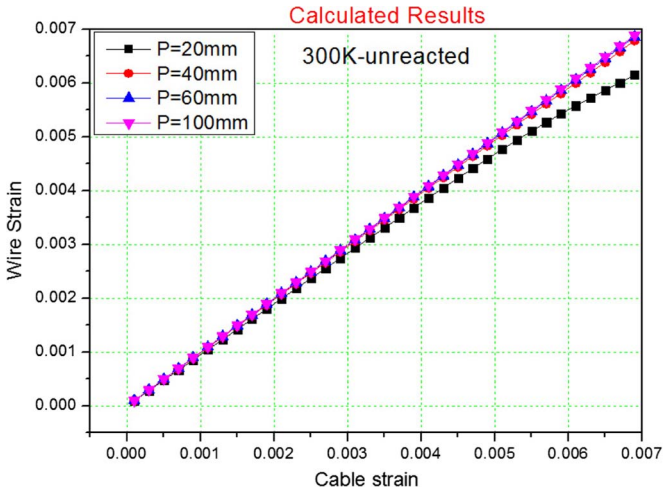

Fig. 11. Wire axial strain versus cable axial strain curves for different pitches at 300 K.

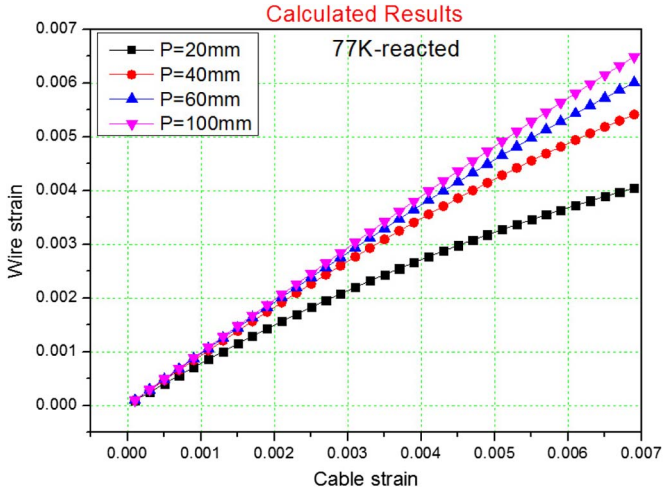

Fig. 12. Wire axial strain versus cable axial strain curves for different pitches at 77 K.

performance degradation. For this reason, special attention was paid to the strain condition of the single wire in different cable configurations. The unreacted wire was considered at 300 K, and the reacted one was considered at 77 and 4.2 K. The fitting functions with exponential type of the stress–strain relation for the reacted wire at 4.2 and 77 K are given as follows.

The fitting function for the reacted wire at 77 K i

$$\sigma(x) = \left(104.42361 - 53.61407e^{\frac{-x}{0.00209}} - 53.61442e^{\frac{-x}{0.00209}}\right) \times 10^6. \quad (24)$$

The fitting function for the reacted wire at 4.2 K is

$$\sigma(x) = \left(147.83979 - 51.87308e^{\frac{-x}{0.00264}} - 98.32292e^{\frac{-x}{0.000741295}}\right) \times 10^6 \quad (25)$$

where σ is the stress (MPa), and x is the strain.

The numerical model was applied to investigate the influence of different cable layouts on the strain distribution when the cable is subjected to axial tensile stress. The simulations are based on data input from the cable and the wire. The cable global axial strain as basic input parameter is corresponding to the axial tension applied to the cable. The wire strain is taken (caused by axial force) along the wire axial direction. The results are shown in Figs. 11–14. It is clear that the cable with a short pitch has a smaller axial wire strain. At 300 K, the difference of wire axial strain among different pitches increases with decreasing temperature; at 300 K, the difference is much smaller than those at 77 and 4.2 K. For long twist pitches (limiting case toward parallel wires), it is found that the wire strain becomes more similar to the cable strain, particularly at 300 K (see Fig. 11). For the cable with a 20-mm-long pitch, the wire strain at 4.2 K is less than at 77 K, as shown in Fig. 14. However, for the cable with a long pitch of 100 mm, the wire strain at 4.2 K evolves similar to the one at 77 K, also shown in Fig. 14.

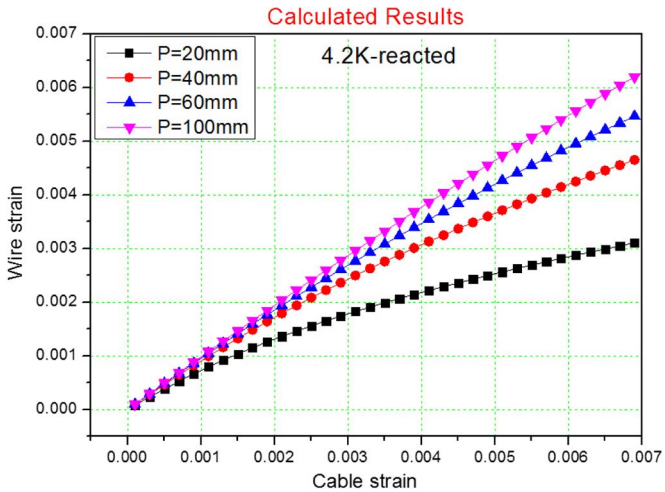

Fig. 13. Wire axial strain versus cable axial strain curves for different pitches at 4.2 K.

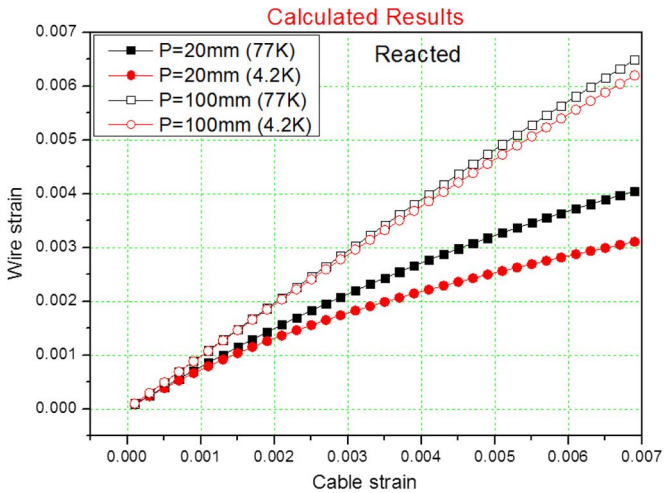

Fig. 14. Wire axial strain versus cable axial strain curves for $p = 20$ and 100 mm at 77 and 4.2 K.

V. Discussion and Conclusion

Most finite-element method mechanical models proposed for numerical analysis on CICC were used to analyze the mechanical behavior of wire and cable and to predict the conductor performance [8], [9]. For a small cable with three twisted single wires, it is not as complicated as for a full-size cable, e.g., ITER toroidal field. The theory of wire rope was used to develop a simple numerical model. The main interest of the model is to investigate the strain of the wires inside cables with different parameters, including the twist pitch and the mechanical properties of the single wire.

The mechanical properties of the single wire are the basic input parameters for the analysis. Both reaction and temperature can influence the wire's strength, because the mechanical properties of the metal components depend on reaction and temperature. Fig. 7 shows that the strength of the reacted Bi2212 wire decreases distinctly compared with that of the unreacted wire. The Ag/Mg alloy is an oxide-dispersion-strengthened alloy, whose mechanical properties should be improved after heat treatment in oxygen. The sharp decline of the strength of Ag may cause a decline in the strength of the entire reacted Bi2212 wire, because Ag comprises a relatively large part of the wire. The strength of the wire increases with decreasing temperature, as shown in Fig. 8. The mechanical property of Bi2212 was mainly confirmed due to its metal components (e.g., Ag and Ag/Mg). In fact, this phenomenon was also observed in titanium and stainless steel alloys such as 316L and 316LN, which has been interpreted by several mechanisms such as deformation twinning, stress-induced transformation, burst dislocation formation, and adiabatic deformation [16]–[19].

The model was first used for comparison with the experimental results in order to evaluate its effectiveness. Because the friction and contact deformation was neglected, there is a little deviation between the numerical and experimental results. However, the main function of the model is to investigate the stress and strain difference among different cable configurations. The modeling results show that the stress required to reach a specific strain increases with enlarging pitch, which is consistent with the experimental results. A more useful analysis on superconducting cables is to investigate the wire axial strain during cooling down and operation, which was simplified here as applying axial tension on the cable. Most studies on the electromechanical properties of the Bi2212 RW were performed at 4.2 and 77 K, and no relevant research was performed on cables. The wire axial strain in altered cable configurations at different temperatures was investigated. It was found that the wire strain increased with enlarged pitch, as shown in Figs. 11–13. Bjoerstad *et al.* reported that the tensile irreversible strain of overpressure-processed Bi2212 wire is around 0.6% [13]. Here, 0.6% was used as a reference to evaluate the cable with a 20-mm-long pitch, as shown in Fig. 14. When the cable strain is 0.6%, the wire strain at 77 and 4.2 K is about 0.37% and 0.3%, respectively. This means that the wire strain is much lower than the applied cable strain. However, for long pitch (e.g., $p = 100$ mm), the wire strain is almost the same as the cable strain, showing no obvious improvement. In addition, the wire axial strain decreases with decreasing temperature for a given applied cable strain, as shown in Fig. 14.

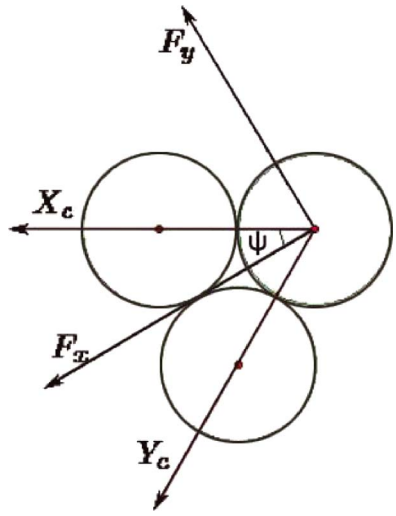

Fig. 15. Contact between wires.

The presented model was used to analyze the strain distribution of a Bi2212 wire in a cable when subjected to tension. During cabling, the tension causing strain on the wire must be well controlled to avoid breakage of the sheath, which could cause leakage during the heat treatment. The model was used to analyze the wire strain distribution under different cabling tensions. The results were used to optimize the cabling technology. The results also illustrate that shorter pitch can reduce the wire axial strain when the cable is under tensile load, which is useful for the optimization of the cable design.

Appendix
Functions of Contact Force

Here, the functions of the contact force are reported. The contact deformation is neglected since it is considered to be small. The contacts of the wire in the cable are shown in Fig. 15.

The equilibrium of the force can be obtained from Fig. 15, i.e.,

$$F_x = X_c \sin\psi + Y_c \sin\psi \tag{A1}$$

$$F_y = X_c \cos\psi - Y_c \cos\psi. \tag{A2}$$

It is assumed that the contact stress is that of two cylindrical bodies in line contact [20]. Hence, the maximum contact stress is given by the equation

$$\sigma_c = -\frac{b}{\Delta} \tag{A3}$$

$$b = \sqrt{\frac{2\left(|X_c| + |Y_c|\right)\Delta}{\pi}} \tag{A4}$$

$$\Delta = 2R\frac{1-\nu^2}{E} \tag{A5}$$

where R is the radius of the wire, E is the Young's modulus, and ν is the Poisson ratio.

REFERENCES

[1] H. Miao, Y. Huang, S. Hong, and J. A. Parrell, "Recent advances in Bi-2212 round wire performance for high field application," *IEEE Trans. Appl. Supercond.*, vol. 23, no. 3, Jun. 2013, Art. no. 6400104.

[2] K. R. Marken, H. Miao, M. Meinesz, B. Czabaj, and S. Hong, "Progress in Bi-2212 wires for high magnetic field applications," *IEEE Trans. Appl. Supercond.*, vol. 16, no. 2, pp. 992–995, Jun. 2006.

[3] T. Hasegawa *et al.*, "HTS conductors for magnets," *IEEE Trans. Appl. Supercond.*, vol. 12, no. 1, pp. 1136–1140, Mar. 2002.

[4] J.-M. Ray, A. Allais, and J.-L. Duchateau *et al.*, "Critical current measurement in HTS Bi2212 ribbons and round wires," *IEEE Trans. Appl. Supercond.*, vol. 19, no. 3, pp. 3088–3093, Jun. 2009.

[5] L. Ye, D. Cruciani, T. Effio, F. Hunte, and J. Schwartz, "The causes of degradation in $Bi_2Sr_2CaCu_2O_{8+x}$ round wires and coils by quenching at 4.2 K," *IEEE Trans. Appl. Supercond.*, vol. 23, no. 5, Oct. 2013, Art. no. 6400811.

[6] P. Bruzzone, K. Sedlak, and B. Stepanov, "High current superconductors for DEMO," *Fusion Eng. Des.*, vol. 88, no. 9/10, pp. 1564–1568, Oct. 2013.

[7] A. Devred *et al.*, "Challenges and status of ITER conductor production," *Supercond. Sci. Technol.*, vol. 27, no. 4, Mar. 2014, Art. no. 044001.

[8] A. S. Nemov, D. P. Boso, I. B. Voynov, A. I. Borovkov, and B. A. Schrefler, "Generalized stiffness coefficients for ITER superconducting cables, direct FE modeling and initial configurations," *Cryogenics*, vol. 50, no. 5, pp. 304–313, May 2010.

[9] H. Bajas, D. Durville, D. Ciazynski, and A. Devred, "Numerical simulation of the mechanical behaviour of ITER cable-in-conduit conductors," *IEEE Trans. Appl. Supercond.*, vol. 20, no. 3, pp. 1467–1470, Jun. 2010.

[10] J. Qin, Y. Wu, L. Warnet, and A. Nijhuis, "A novel numerical mechanical model for the stress–strain distribution in superconducting cable-in-conduit conductors," *Supercond. Sci. Technol.*, vol. 24, no. 6, Apr. 2011, Art. no. 065012.

[11] X. F. Lu, N. Cheggour, T. C. Stauffer, and C. C. Clickner, "Electromechanical characterization of Bi-2212 strands," *IEEE Trans. Appl. Supercond.*, vol. 21, no. 3, pp. 3086–3089, Jun. 2011.

[12] P. Tixador, C. E. Bruzek, B. Vincent, A. Malgoli, and X. Chaud, "Mechanically reinforced Bi-2212 strand," *IEEE Trans. Appl. Supercond.*, vol. 25, no. 3, Jun. 2015, Art. no. 6400404.

[13] R. Bjoerstad *et al.*, "Strain induced irreversible critical current degradation in highly dense Bi-2212 round wire," *Supercond. Sci. Technol.*, vol. 28, no. 6, Apr. 2015, Art. no. 062002.

[14] G. A. Costello, *Theory of Strand Rope*, 2nd ed. New York, NY, USA: Springer Verlag, 1997.

[15] C. Dai *et al.*, "The axial tensile stress–strain characterization of Ag-sheathed Bi2212 round wire," *IEEE Trans. Appl. Supercond.*, vol. 25, no. 3, Jun. 2015, Art. no. 6400304.

[16] N. C. van den Eijnden, A. Nijhuis, Y. IIyin, W. A. J. Wessel, and H. H. J. ten Kate, "Axial tensile stress–strain characterization of ITER model coil type Nb_3Sn strands in TARSIS," *Supercond. Sci. Technol.*, vol. 18, no. 11, pp. 1523–1532, Oct. 2005.

[17] A. Kajbafvala *et al.*, "Dispersion-strengthened silver alumina for sheathing $Bi_2Sr_2CaCu_2O_{8+x}$ multifilamentary wire," *IEEE Trans. Appl. Supercond.*, vol. 22, no. 1, Feb. 2012, Art. no. 8400210.

[18] O. P. Anashkin *et al.*, "Tensile tests of ITER TF conductors jacket materials," in *Proc. AIP Conf.*, 2012, vol. 1435, pp. 117–124.

[19] H. J. Liu, Y. Wu, Q. Y. Han, Z. X. Wu, and L. F. Li, "Mechanical tests on the ITER PF 316L jacket after compaction," *Croygenics*, vol. 51, no. 6, pp. 234–236, Jun. 2011.

[20] K. L. Johnson, *Contact Mechanics*. Cambridge, U.K.: Cambridge Univ. Press, 1985.

Authors' biographies not available at the time of publication.